Impact of fuel composition on the recirculation zone structure and its role in lean premixed flame anchoring

Seunghyuck Hong, Santosh J. Shanbhogue, Ahmed F. Ghoniem [*]

Reacting Gas Dynamics Laboratory, Center for Energy and Propulsion Research, Department of Mechanical Engineering, Massachusetts Institute of Technology, 77 Massachusetts Avenue, Cambridge, MA 02139, United States

Available online 26 June 2014

Abstract

We investigate the dependence of the recirculation zone (RZ) size and structure on the fuel composition using high-speed particle image velocimetry (PIV) and chemiluminescence measurements for C_3H_8/H_2/air lean premixed flames stabilized in a backward-facing step combustor. Results show an intricate coupling between the flame anchoring and the RZ structure and length. For a fixed fuel composition, at relatively low equivalence ratios, the time-averaged RZ is comprised of two counter rotating eddies: a primary eddy (PE) between the shear layer and the bottom wall; and a secondary eddy (SE) between the vertical step wall and the PE. The flame stabilizes downstream of the saddle point of the dividing streamline between the two eddies. As equivalence ratio is raised, the flame moves upstream, pushing the saddle point with it and reducing the size of the SE. Higher temperature of the products reduces the velocity gradient in the shear layer and thus the reattachment length. As equivalence ratio approaches a critical value, the saddle point reaches the step and the SE collapses while the flame starts to exhibit periodic flapping motions, suggesting a correlation between the RZ structure and flame anchoring. The overall trend in the flow field is the same as we add hydrogen to the fuel at a fixed equivalence ratio, demonstrating the impact of fuel composition on the flow field. We show that the reattachment lengths (L_R), which are shown to encapsulate the mean RZ structure, measured over a range of fuel composition and equivalence ratio collapse if plotted against the strained consumption speed (S_c). Results indicate that for the flame to remain anchored, the RZ structure should satisfy $\frac{L_{R,isothermal}}{L_{R,reacting}} \cdot \frac{S_c}{U_\infty} \sim 0.1$. If this criterion cannot be met, the flame blows off, flashes back or becomes thermoacoustically unstable, suggesting a Damköhler-like criterion for aerodynamic flame stabilization in backward-facing step flows.

Keywords: Particle image velocimetry (PIV); Recirculation zone length; Backward-facing step; Strained consumption speed; Flame anchoring

* Corresponding author. Address: 77 Massachusetts Avenue, Room 3-344, Cambridge, MA 02139, United States. Fax: +1 617 253 5981.
   E-mail address: ghoniem@mit.edu (A.F. Ghoniem).

1. Introduction

Recirculation zones are ubiquitous features in many combustion systems. In aircraft and

power-plant combustors, they are pivotal for aerodynamic stabilization of flames, providing both a low-velocity zone and a pool of radicals and hot products without incurring high pressure losses. In solid-fuel combustion systems such as entrained-flow pulverized coal gasifiers, they are used for recirculating hot products to aid in feed-stock ignition. Recirculation zones (RZ's) are induced using a variety of flow features, e.g., sudden expansions, bluff bodies, a combination of domes and swirlers, where they form as a result of flow-separation processes, except the one in swirling flows that form as a result of vortex breakdown, and adverse pressure gradients.

The dimension of the RZ is a critical input parameter in a number of reduced order models and non-dimensional numbers. In reactor-network models, RZ's are modeled as perfectly-stirred reactors where the volume is inversely related to the characteristic residence time [1]. In reduced order models of entrained flow gasifiers, the RZ length is used as an input to predict species concentrations [2]. Flame blowout models for gas-turbines, based on the Damköhler number ($\tau_{\mathrm{flow}}/\tau_{\mathrm{chem}}$), often use the RZ length as a characteristic length scale of flows [3]. Some combustion-chambers are designed with a fixed RZ size. In a trapped vortex combustor, for instance, the streamwise length of the RZ is bound by the geometry of the cavity. In all other configurations, the RZ "floats," where its dimensions exhibit strong sensitivities to flow parameters (e.g., velocity, Reynolds number, turbulent intensities), geometrical features (e.g., blockage, corner sharpness) and combustion related parameters such as equivalence ratio and preheat temperature [4–6].

This study focuses on the dependence of the size and structure of RZ on the fuel characteristics and heat release and how it aids in flame anchoring. The objective is to gain insight into the physical processes underlying aerodynamic flame stabilization and improve the predictive capabilities of reduced order models.

1.1. Basic parametric dependencies of the recirculation zone

In backward-facing step (non-reacting) flows, RZ's form around $Re_H \sim \mathcal{O}(1)$ (where Re_H is the Reynolds number based on the step height, H) as inertial forces start to grow. As Re_H is raised in the laminar regime, its downstream extent (denoted by L_R hereafter) increases almost linearly until the flow starts to transition to turbulence [4,7,8]. If Re_H is raised further, the flow becomes unsteady, shedding vortices, which reduces the average value of L_R until the flow becomes fully turbulent where L_R becomes nearly constant. At a fixed Re_H, L_R depends on the inlet flow profile (i.e., the nature of the inlet boundary layer and turbulent intensities) and geometrical parameters

(e.g., the aspect ratio) [6]. For a given Re_H, higher turbulent intensities in the inlet flow cause L_R to decrease [9] suggesting that the RZ could be a potential surrogate marker for the inflow turbulence.

Studies that previously examined the effect of combustion on the RZ commonly found that exothermic processes reduce L_R [10–12], attributing this to the flow acceleration associated with gas expansion, which reduces the shear, causing the shear layer to reattach earlier downstream.

1.2. Focus of this study

In this study, we investigate the dependence of L_R on the fuel composition and equivalence ratio, with the intent to uncover the role of RZ's in flame anchoring. Previous studies [10–12] examined the impact of combustion, and found significant changes in the velocity field for a single fuel (mostly at one equivalence ratio) using multi-point LDV measurements. We vary the fuel mixtures using hydrocarbons and hydrogen. Hydrogen addition slightly changes flame temperatures, but dramatically speeds up the kinetics, an impact of which has not been studied before. We also use high-speed particle image velocimetry (PIV) to reveal the subtle impact of combustion on the RZ structure.

Flame anchoring has been approached in the past by looking at the stability boundaries, i.e., the blow-off [3] and the flashback limits [13]. This paper discusses mechanistically the interaction of the flame with the RZ between these boundaries, using the flame images and the PIV data obtained over a range of equivalence ratios and fuel compositions. We demonstrate that the structure and size of the RZ are strongly correlated with the flame stability characteristics.

2. Experimental setup

This section provides key information on the experimental setup; more detailed description can be found in Ref. [14].[1] The schematic of the combustor test section is shown in Fig. 1. The combustor duct made of stainless steel has a rectangular cross-section 40 mm high and 160 mm wide. The air inlet is choked and the combustor exit is open to ambient air. A honeycomb-shaped flow straightener is installed at 0.3 m downstream the choke plate to reduce the inlet turbulent intensity, which was maintained at $u'_{\mathrm{rms}} \sim 0.3$ m/s ($\sim 6\%$ of the mean). The step height is 20 mm, located ~ 0.98 m downstream the choke plate.

---

[1] Note that the combustor length was shortened significantly to reduce the chances for early acoustic coupling.

Quartz windows are installed in the vicinity of the step, providing optical access. The overall length of the combustor is ~1.5 m.

Fuel is injected 0.02 m downstream of the choke plate. A pair of Sierra C100M Smart-Trak digital mass flow controllers is used to control the flow rates of propane and hydrogen, leading to the accuracy of equivalence ratio measurements of $\Delta\phi \sim 0.002$. Pressure is measured at 0.20 m upstream of the sudden expansion using a flush-mounted, water-cooled Kistler 7061B pressure sensor, which is sampled at 10 kHz. High-speed, spatially resolved chemiluminescence images of the flame are obtained using a 12-bit 1280×1024 NAC GX-1 high-speed CMOS camera with an F-mount Nikon 60-mm $f/2.8$ micro-lens, at a rate of 500 Hz. A 1-mm BG-39 optical colored glass filter is placed in front of the camera to reduce IR radiation from the flame. All data are acquired using a National Instruments PCIe-6259 data acquisition board with a custom Matlab code.

Planar velocity fields are obtained using PIV measurements. The details of the setup (e.g., laser, optics, seeding) are described in Ref. [14]. The light source consists of a 527 nm Nd:YLF laser producing dual pulses at a rate up to 5 kHz with

a peak power output of 25 mJ/pulse. The interval between the laser pulses was set to 80–150 μs depending on the field of view. The same camera and lens used for flame imaging are used for PIV, with an aperture of $f/8$ at a rate of 1 kHz. The field of view is set to 65–120 mm in the streamwise direction depending on the operating conditions, which corresponds to 0.05–0.1 mm/pixel. The LaVision DaVis 7.2 software is used to process the 1280×1024 pixel images of the seeding particles, using a multi-pass approach with the final pass of a 32×32 pixel window with 50% overlap, producing velocity fields with a spatial resolution of 0.8–1.5 mm.

3. Results and discussion

The combustor was operated at atmospheric pressure and at a constant Reynolds number of 6500 based on the step height (20 mm). The plug flow velocity is ~5.2 m/s at 300 K, which varies by less than ~10% across all the tests.

We obtained flame images and PIV fields for C_3H_8:H_2 volume ratios corresponding to 50:50, 70:30, and 100:0, for a range of equivalence ratios in increments of 0.03–0.06 while the combustor is stable, as discussed in Section 3.1. We note that the effective Lewis number is greater than unity for all the fuel blends considered herein [15], and thus we do not expect significant thermo-diffusive effects for the parametric space of conditions in this paper.

3.1. Operating regimes

We first define the conditions where we examine the RZ. Figure 2 shows the overall sound pressure level (OASPL) as a function of the equivalence ratio (ϕ) for different hydrogen concentration in the fuel (X_{H_2}). The OASPL is defined as:

$$\text{OASPL (dB)} = 10\log_{10}\overline{\left[\frac{p(t) - \overline{p(t)}}{p_0}\right]^2} \qquad (1)$$

where overbars indicate average values, $p(t)$ is the pressure measured in an interval $t_1 < t < t_2$ while the operating conditions are constant and $p_0 = 2 \times 10^{-5}$ Pa is the standard acoustic reference pressure for air. The combustor operation is limited by the two stability limits: lean blow-off and flashback. The latter occurs at relatively high ϕ's above which the flame flashes back toward the inlet section upstream, while the former defines the lower boundary of ϕ below which the flame escapes downstream.

In between, we observe two distinct regimes: (1) one at lower ϕ's where the pressure amplitude is very low, corresponding to broadband noise, referred to as 'Zone I' and (2) another closer to
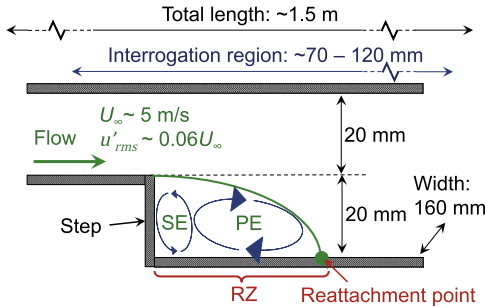

Fig. 1. Schematic of the combustor test section. The recirculation zone (RZ) is comprised of two large eddies: a primary eddy (PE) and secondary eddy (SE), as discussed in Section 3.3.
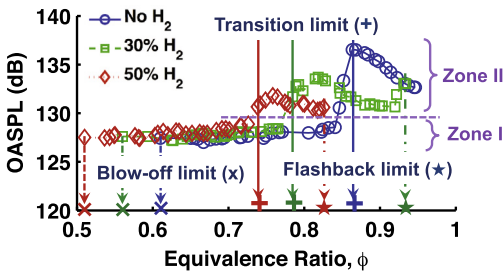

Fig. 2. Overall sound pressure level as a function of equivalence ratio for different mixture compositions (indicated by volume) of C_3H_8/H_2/air flames. $T_{in} = 300$ K and $Re = 6500$ for all cases.
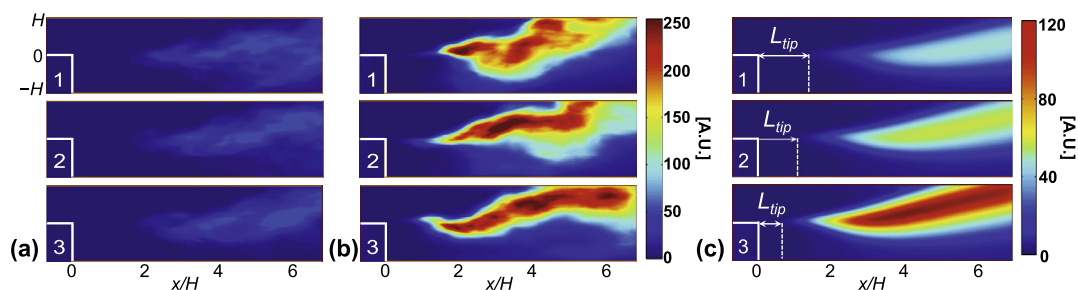
Fig. 3. High-speed chemiluminescence images (4 ms between frames) are shown for (a) $\phi = 0.75$ and (b) $\phi = 0.95$ (both C_3H_8/air flames), representative of Zone I and II, respectively. (c) The time-averaged chemiluminescence intensity contour at (1) $\phi = 0.75$, (2) $\phi = 0.79$ and (3) $\phi = 0.85$ for C_3H_8/air flames. The flame tip location (L_{tip}) is determined using the same absolute level ($\sim$4 a.u.). The field of view covers $\sim$6.8H downstream the step, where H denotes the step height, 20 mm.

the flashback limit, where low pressure amplitude[2] with a peak at $\sim$70 Hz is observed, referred to as 'Zone II.' To illustrate, we present in Fig. 3a and b high-speed chemiluminescence images representative of each zone, recorded at $\phi = 0.75$ and 0.95, respectively, for propane/air mixtures. The figures show that the flame is stabilized in a reacting shear layer and relatively 'stable' in Zone I, whereas in Zone II, while the flame does not flash back toward upstream the step, it exhibits weak periodic flapping motions associated with large vortices.[3] We refer to the boundary at which the combustor transitions from Zone I to Zone II as the 'transition limit.'

The hydrogen addition shifts the operating boundaries of all three limits – the blow-off, transition and flashback limits – to leaner conditions, while maintaining the same regimes in between. In addition, as X_{H_2} is raised, the pressure amplitude in Zone II decreases while we observe similar flame flapping motions at the same frequency.

In what follows, we discuss flame images and PIV data obtained in Zone I – between the lean blow-off and transition limits – as illustrated in Fig. 2. These limits are consistent within the range of $\Delta\phi \sim 0.01 - 0.02$ as we repeat experiments. The spectral content of the dynamic pressure measurements ensured that there are no acoustically coupled oscillations for all test conditions (in Zone I).

3.2. Mean flame images

Here, we examine the overall location and shape of the flame envelope under different conditions. The time-averaged chemiluminescence intensity contours are shown in Fig. 3c for

propane/air mixtures at $\phi = $ (1) 0.75; (2) 0.79; and (3) 0.85. The flame tip locations, where the upper- and lower-edges of the flame envelope intersect, are defined using the same absolute intensity level corresponding to 3% of the maximum intensity at $\phi = 0.88$, which are used to examine 'relative' positions of the flames of different mixtures.

As the equivalence ratio is raised, the chemiluminescence intensity becomes brighter because of the higher heat release, while the overall flame tip location moves upstream toward the step with larger angle with respect to the incoming flow, mainly attributed to an increase in the burning velocity. The changes in the locations of the flame tip and envelopes (e.g., see Fig. 4) with respect to the RZ are discussed in Section 3.3.2.

3.3. Streamlines and vorticity field

The time-resolved PIV data reveal unsteady flow features in the shear layer, e.g., shedding and convection of small vortices and their pairing events at some instances (see [14] for example). While the instantaneous images depict the evolution of the unsteady flow field, the large-scale structures (e.g., RZ's) vary from one instant to another. To quantify the size, location and vorticity of the RZ's as well as their dependence on the fuel composition and equivalence ratio, we examine the time-averaged PIV data in what follows.

3.3.1. Impact of equivalence ratio on the flow field

Figure 4 shows the mean flow field for propane/air mixtures ($X_{H_2} = 0\%$) at $\phi = $ (a) 0.72, (b) 0.79 and (c) 0.88. Streamlines-based arrows depict the direction of the flow and the color shown in the top bar illustrates the vorticity field. The vorticity is calculated from the velocity vectors in adjacent grid points using a second-order central difference scheme. In Fig. 4a, we observe two eddies within the RZ: a primary eddy (PE) between the shear layer and the bottom wall,

---

[2] The pressure amplitude is low as compared to the case of a longer combustor presented in [14,16].

[3] The mechanism of the instability is discussed in our prior studies [14,16].
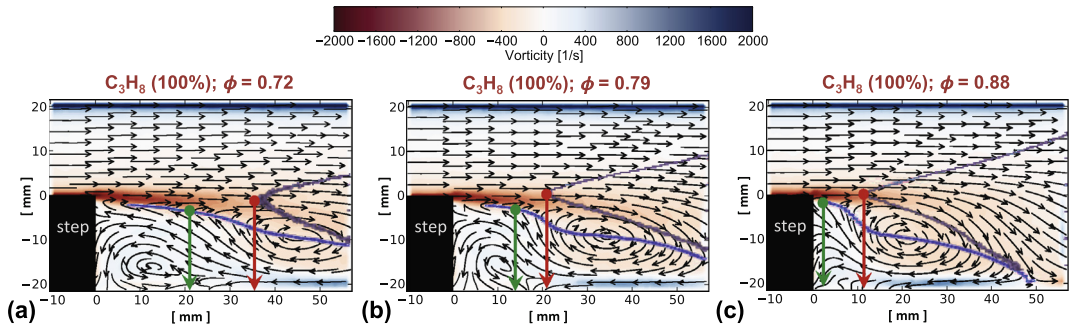
Fig. 4. The time-averaged PIV data are shown for (a) $\phi = 0.72$; (b) $\phi = 0.79$; and (c) $\phi = 0.88$ for C_3H_8/air mixtures. The mean flame envelopes (lavender lines) are superimposed. The zero streamwise-velocity contours are indicated by blue lines. The axial locations of the saddle point and flame tip are marked by green and red arrows, respectively. (For interpretation of the references to colour in this figure legend, the reader is referred to the web version of this article.)

exhibiting negative vorticity; and a secondary eddy (SE) rotating in the opposite direction between the PE and the vertical step wall. The strongest vorticity is observed near the edge of the step, which decreases downstream of the shear layer. The blue lines shown in the figure indicate the zero streamwise-velocity contours, which are used to quantify the reattachment length for a range of conditions in Section 3.4.

At higher ϕ's, the PE becomes more compact, moving upstream closer to the step, while the SE is reduced in size, almost collapsing at $\phi = 0.88$ (Fig. 4c). It is evident from Fig. 4 that the flow field is significantly impacted by ϕ.

These observations agree with previous studies [10,12], which compare reacting and non-reacting flows, showing the former to have shorter but more intense RZ's due to the gas expansion associated with heat release. As ϕ is raised, the temperature (density) jump across the flame becomes more significant, raising the velocity and reducing the shear. The observations so far suggest that the change in the RZ structure and size is a function of the temperature ratio across the flame.

In the next section, we further examine Fig. 4 to discuss the observed change in the flow field in relation to the overall flame location.

3.3.2. The recirculation zone and flame tip locations

In Fig. 4a–c, the two superimposed lavender lines indicate the corresponding mean flame envelope, determined from the chemiluminescence intensity contours (e.g., Fig. 3c) as described in Section 3.2. The saddle point where separating streamlines between the two eddies intersect with the zero streamwise-velocity line is marked by green dot, while the flame tip is indicated by red dot. For all ϕ's, we observe a similar relative position of the flame with respect to the RZ. The flame tip is located downstream of the saddle point, indicating that the flame is stabilized in the low-velocity region formed by recirculating flows in the shear layer. The lower-edge of the flame

envelope lies between the center and the top-edge of the PE.

Figure 5 plots the axial locations (from the step) of the saddle point and the flame tip for a range of ϕ for propane/air mixtures ($X_{H_2} = 0\%$). The figure shows that as ϕ increases, the saddle point gradually approaches the step, reaching it at $\phi = 0.88$, while the flame tip also moves upstream, located certain distance downstream of the saddle point. Figures 2, 4 and 5 collectively show that the transition limit ($\phi \approx 0.88$), at which the flame starts to exhibit periodic flapping motions, coincides with the moment when the saddle point reaches the step and the SE collapses, suggesting that the change in the RZ structure is correlated with the flame stability near the anchoring region. This will further be discussed in Section 3.5.

3.3.3. Impact of hydrogen addition on the flow field

Next, we examine the impact of the fuel composition on the RZ structure and size. Figure 6 shows the time-averaged PIV fields for $X_{H_2} =$ (a) 30% and (b) 50% (by volume) both at $\phi = 0.72$. See Fig. 4a for $X_{H_2} = 0\%$ case at the same ϕ. The equilibrium burnt gas temperatures for the three cases are ~1920, 1927 and 1914 K, respectively. Despite the similar temperatures,
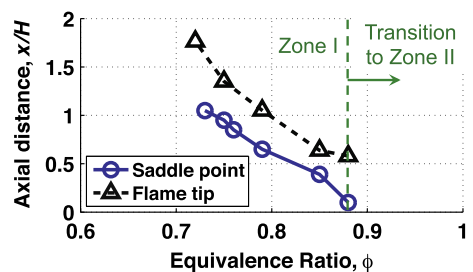

Fig. 5. The axial locations of the saddle point and flame tip estimated over a range of ϕ for C_3H_8/air mixtures.
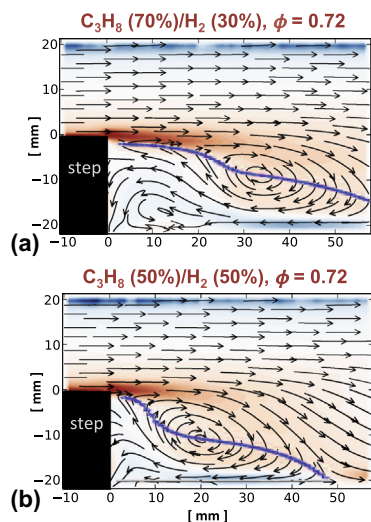
Fig. 6. The time-averaged PIV data for (a) C_3H_8 (70%)/H_2 (30%); (b) C_3H_8 (50%)/H_2 (50%) (volume ratio). For both cases, $\phi = 0.72$. The vorticity scale and blue line denote the same as Fig. 4. (For interpretation of the references to colour in this figure legend, the reader is referred to the web version of this article.)

the flow field is significantly impacted by X_{H_2}. As X_{H_2} increases, the PE moves closer to the step while the SE becomes smaller, similar to those observed at a higher equivalence ratio for propane/air mixtures.

These observations are consistent across all equivalence ratios and propane/hydrogen blends we tested. Addition of hydrogen at a given ϕ does little to the burned gas temperature, but significantly changes the RZ structure, suggesting that the changes in the flow-field are not solely determined by the temperature difference across the flame.

3.4. Recirculation zone structure and reattachment length

Here, we examine zero streamwise-velocity contours (blue lines in Figs. 4 and 6) for a range of ϕ and X_{H_2}, which are representative of the RZ structure. For example, Fig. 4 depicts that the blue lines pass through the saddle point and the center of the PE for all conditions. The slope of the line between the two locations becomes steeper as the PE moves closer to the step and the SE becomes smaller (at higher ϕ). The flow reattachment point is also marked by the blue line where it intersects with the bottom wall (see Fig. 4c).

Figure 7 shows the zero streamwise-velocity lines for selected conditions, illustrating the impact of ϕ and X_{H_2} on the mean flow field. As ϕ is raised for a given X_{H_2}, L_R gradually decreases. The location of the kink within $-0.5 < y/H < 0$ indicates that the PE moves

upstream at a higher equivalence ratio. At a fixed ϕ (e.g., 0.72), as X_{H_2} increases from 0% to 30% and 50%, the similar trends are observed.

The overlapped lines (circled in Fig. 7), e.g., three cases corresponding to $L_R/H \sim 2.4$ and two cases corresponding to $L_R/H \sim 3$, indicate that the overall mean flow structures are the same among different mixtures if they have the same reattachment length, demonstrating that the streamwise variation and structure of the mean flow field is encapsulated in L_R.

Next, we use the zero streamwise-velocity lines to quantify the reattachment length, L_R, i.e., the axial distance between the reattachment point and the step. If the reattachment point is not captured within the field of view for PIV measurements, we extrapolate these curves. In Fig. 8, we plot L_R measured over a range of ϕ and X_{H_2}. We normalize L_R by both the step-height (H) and the reattachment length measured for the corresponding non-reacting flow ($L_{cold} \sim 7H$). The instantaneous PIV data (not presented) show that the unsteadiness of the flow causes the reattachment point to fluctuate within $\pm 0.5H$ in all conditions. Figure 8 shows that an exothermic process reduces L_R by 20–65% depending on the operating conditions as compared to its counterpart of the non-reacting flow, consistent with previous studies [10–12]. We observe that L_R decreases almost linearly with increasing ϕ while also becoming shorter for higher X_{H_2}, suggesting a correlation between the reattachment length and the consumption speed. This is further examined next.

3.5. Correlating the reattachment length with the flame stability regimes

Our prior studies [14,16] demonstrated that the strained consumption speed can be used to collapse the scatter of the mode-transitions observed over a range of mixture compositions and inlet
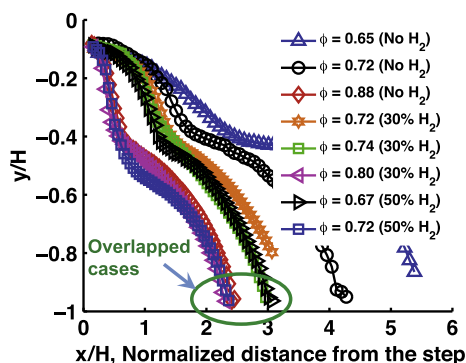

Fig. 7. The zero streamwise-velocity contours (the same as blue lines shown in Figs. 4 and 6) for selected combinations of ϕ and X_{H_2}. (For interpretation of the references to colour in this figure legend, the reader is referred to the web version of this article.)
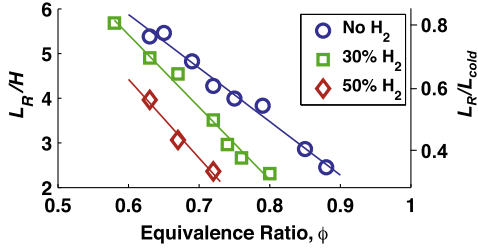
Fig. 8. The normalized reattachment length as a function of ϕ for different X_{H_2}.

temperatures. In this section, we attempt to correlate the reattachment length with the consumption speed.

We use an in-house opposed flow strained flame model [17,18] to compute the consumption speed, defined as:

$$S_c = \frac{\int_{-\infty}^{\infty} q''' / c_p dy}{\rho_u (T_b - T_u)} \quad (2)$$

where q''' is volumetric heat release rate; c_p is specific heat of the mixture; y is the coordinate normal to the flame; ρ_u is density of unburned mixture; T_u and T_b are unburned and burned gas temperatures, respectively. The consumption speed is calculated based on characteristic stretch rates of 180–280 s^{-1}, which are representative of the conditions used in this paper, as documented in detail in Hong et al. [14,16]. The thermochemical properties of mixtures are provided by Cantera [19] using the GRI-Mech. 3.0 kinetic model. More details of the strained flame model and the numerical method can be found in Refs. [17,18].

Figure 9a plots L_R as a function of S_c (normalized by the approach flow velocity, U_∞). The three lines (each for a fixed mixture composition) shown in Fig. 8 collapse onto a single characteristic line, demonstrating that the size and structure of RZ's formed over a backward-facing step are a function of the consumption speed, rather than a temperature jump across the flame as suggested previously.

In Fig. 9b, we also plot the OASPL against the normalized consumption speed. The figure shows that the scatter of the stability- and transition-limits defined for different mixture compositions (see Fig. 2) are all collapsed using the same parameter, demonstrating that the strained consumption speed is a governing parameter determining the overall stability characteristics.

Figure 9 indicates that the size and structure of the RZ, which are a function of the strained consumption speed only, correlate well with flame stability characteristics. For mixtures with high consumption speeds, for example, the overall flame envelope moves upstream (see Fig. 3c) while the RZ structure changes such that L_R decreases along the characteristic line shown in Fig. 9a. When L_R is reduced to a critical value, e.g., ~35% of L_{cold}, the saddle point between the two
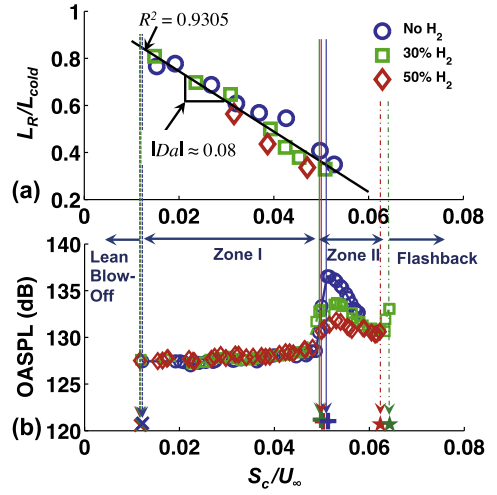

Fig. 9. (a) The normalized reattachment lengths and (b) the OASPL (overall sound pressure level, see Eq. (1)), the same data shown in Figs. 8 and 2, respectively, as a function of the normalized consumption speed. A linear fit and the reciprocal of the slope is shown in (a).

eddies in the RZ reaches the step (see Fig. 5) and the SE almost collapses (see Figs. 4c or 6b). Beyond this point, the system becomes susceptible to thermoacoustic coupling, starting to exhibit weak pressure fluctuations along with periodic flame flapping motions.

In Fig. 9a, we note that the reciprocal of the slope resembles a Damköhler number (Da). The slope of the characteristic line, $|(L_R/L_{cold})/(S_c/U_\infty)|$, is a ratio of chemical time scale and flow time scale. The flow length scale is taken here as the reattachment length of the non-reacting flow (L_{cold}) because it is representative of the baseline flow characteristics that capture the effect of geometry and inlet flow conditions. Its counterpart of the combustion process is represented here by L_R, which strongly depends on the fuel composition and equivalence ratio. The data show that across a range of ϕ and X_{H_2}, $Da \equiv |(L_{cold}/U_\infty)/(L_R/S_c)| = \tau_{flow}/\tau_{chem} \sim 0.1$. We note that $Da \ll 1$ is attributed to the fact that a length scale chosen here for flames is the reattachment length that is order(s) of magnitude higher than a commonly used length scale, e.g., flame thickness. This parameter encapsulates the coupled interaction between the flame and the flow that maintains a stable combustion over a backward-facing step, where the flame adjusts its anchoring point in accordance with the change in the RZ structure and size such that $Da \sim 0.1$.

4. Concluding remarks

In this study, we examined the impact of fuel characteristics on the recirculation zone (RZ)

formed over a backward-facing step under lean premixed condition using high-speed PIV and flame chemiluminescence measurements over a range of equivalence ratios (ϕ) and fuel compositions (X_{H_2}).

Results indicate that the size and structure of the RZ are strongly correlated with the overall flame stability characteristics across a range of the combustion parameters (e.g., ϕ, X_{H_2}). As ϕ or X_{H_2} is raised, the primary eddy (PE) becomes more compact and moves upstream, reducing the size of the secondary eddy (SE) and the reattachment length (L_R), while the relative position of the RZ with respect to the mean flame envelope remains nearly the same. We observe that as ϕ approaches a critical value (i.e., the transition limit) at which the combustor transitions to a thermoacoustic instability, the saddle point (near the left-edge of the PE) reaches the step and the SE almost collapses.

We demonstrated that (1) the dependence of the mean RZ structure – shown to be represented by L_R and the zero streamwise-velocity contours – on X_{H_2} and ϕ can be expressed as a function of the strained consumption speed of the inlet mixture alone, and that (2) the consumption speed also correlates well with the lean blow-off, transition and flashback limits observed for different mixture compositions. These results highlight a critical role of the RZ in the overall stability and flame anchoring as well as its impact on the susceptibility of the system to thermoacoustic coupling, where underlying the critical values of the consumption speed defining the stability- and transition-limits are the RZ structure and size that change in ways conducive for stable flame anchoring.

The results presented herein also have significant implications for studies that investigate hydrodynamic stability characteristics (see [20,21] for examples). These stability analyses typically assume that the velocity and temperature fields are independent of each other, or at the very least, independent of kinetic processes. The results represented by Fig. 9 imply that changes in the velocity field are strongly coupled to changes in the kinetics as well as the temperature field. It will be interesting to examine the impact of these coupled interactions, e.g., on the stability curves in [20].

References

[1] L.S. Pedersen, P. Breithauptb, K.D. Johansen, R. Weber, *Combust. Sci. Technol.* 127 (1997) 251–273.
[2] R.F. Monaghan, A.F. Ghoniem, *Fuel* 91 (2012) 61–80.
[3] S.J. Shanbhogue, S. Husain, T. Lieuwen, *Prog. Energy Combust. Sci.* 35 (2009) 98–120.
[4] A.F. Ghoniem, Y. Cagnon, *J. Comput. Phys.* 68 (1987) 346–377.
[5] J.C. Pan, M.D. Vangsness, D.R. Ballal, *J. Eng. Gas Turb. Power* 114 (1992) 783–789.
[6] J. Eaton, J. Johnston, *AIAA J.* 19 (1981) 1093–1100.
[7] B.F. Armaly, F. Durst, J.C.F. Pereira, B. Schönung, *J. Fluid Mech.* 127 (1983) 473–496.
[8] J.A. Sethian, A.F. Ghoniem, *J. Comput. Phys.* 74 (1988) 283–317.
[9] H. Park, W.-P. Jeon, H. Choi, J.Y. Yoo, *Phys. Fluids* 19 (2007) 105103.
[10] R.W. Pitz, J.W. Daily, *AIAA J.* 21 (1983) 1565–1570.
[11] R.D. Gould, W.H. Stevenson, H.D. Thompson , *J. Propul. Power* 10 (1994) 639–645.
[12] R.S. Gabruk, L.A. Roe, *J. Propul. Power* 10 (1994) 148–154.
[13] T. Lieuwen, V. McDonell, E. Petersen, D. Santavicca, *J. Eng. Gas Turb. Power* 130 (2008) 11506.
[14] S. Hong, R.L. Speth, S.J. Shanbhogue, A.F. Ghoniem, *Combust. Flame* 160 (2013) 1381–1397.
[15] R.L. Speth, Fundamental Studies in Hydrogen-Rich Combustion: Instability Mechanisms and Dynamic Mode Selection, Ph.D. Thesis, Massachusetts Institute of Technology, 2010.
[16] S. Hong, S.J. Shanbhogue, R.L. Speth, A.F. Ghoniem, *Combust. Flame* 160 (2013) 2827–2842.
[17] R.L. Speth, Y.M. Marzouk, A.F. Ghoniem, 43th AIAA Aerospace Sciences Meeting and Exhibit, Paper No. 2005-143, 2005.
[18] Y.M. Marzouk, A.F. Ghoniem, H.N. Najm, *AIAA J.* 41 (2003) 641–652.
[19] D. Goodwin, Cantera: object-oriented software for reacting flows, 2005.
[20] D. Wee, T. Yi, A. Annaswamy, A.F. Ghoniem, *Phys. Fluids* 16 (2004) 3361–3373.
[21] B. Emerson, J. O'Connor, M. Juniper, T. Lieuwen, *J. Fluid Mech.* 706 (2012) 219–250.